BULLETIN OF THE POLISH ACADEMY OF SCIENCES
TECHNICAL SCIENCES, Vol. 72(1), 2024, Article number: e148835
DOI: 10.24425/bpasts.2024.148835

Can data processing algorithms ensure sufficient accuracy to estimate human body pose via wearable systems with use of IMU sensors? – an experimental evaluation

Aleksandra SZCZERBA, Piotr PROCHOR*, and Szczepan PISZCZATOWSKI

Department of Biomaterials and Medical Devices Engineering, Institute of Biomedical Engineering, Faculty of Mechanical Engineering, Bialystok University of Technology, Wiejska 45C Street, 15-351 Bialystok, Poland

Abstract. Background: The aim of the study was to answer two questions: 1 – Can data processing algorithms ensure sufficient accuracy for estimating human body pose via wearable systems? 2 – How to process the IMU sensor data to obtain the most accurate information on the human body pose? To answer these questions, the authors evaluated proposed algorithms in terms of accuracy and reliability. Methodology: data acquisition was performed with a tested IMU sensors system mounted onto a Biodex System device. Research included pendulum movement with seven angular velocities (10–120°/s) in five angular movement ranges (30–120°). Algorithms used data from accelerometers and gyroscopes and considered complementary and/or Kalman filters with adjusted parameters. Moreover, angular velocity registration quality was also taken into consideration. Results: differences between means for angular velocity were 0.55÷1.05°/s and 1.76÷3.11%. In the case of angular position relative error of means was 4.77÷10.84%, relative error of extreme values was 2.15÷4.81% and Spearman's correlation coefficient was 0.74÷0.89. Conclusions: the algorithm calculating angles based on acceleration-derived quaternions and with the implementation of a Kalman filter was the most accurate for data processing and can be adapted for future work with IMU sensors systems, especially in wearable devices that are designated to support humans in daily activity.

Keywords: pose estimation; wearable electronics; motion sensors; inertial measurement unit; human motion tracking.

1. INTRODUCTION

Wearable electronics are very promising tools in fields concerning human activity such as clinical gait analysis [1], sport biomechanics [2, 3] or rehabilitation [4]. One of the prospective uses of wearable devices is to monitor the elderly in their daily environment [5], which can ensure *inter alia* the possibility of remote fall detection. Recently, this equipment has become more popular in the research on human daily physical activity [6] due to its low-cost and size as well as – which is probably even more important – the possibility to expand research space beyond the laboratory.

There are several parameters that can be registered, analyzed or transmitted via wearable electronics [7], among which one can distinguish kinematic data, crucial in fall detection studies [8]. For the purpose of kinematic analyses, inertial measurement unit (IMU) sensors are the most commonly used for data acquisition [9, 10]. These sensors are used in the research on human daily physical activity [11, 12] and allow to obtain data directly connected with pose estimation, such as roll and pitch angles [13]. However, IMU sensors are not able to directly obtain data referring to a position of the examined object without hardware calibration and implementation of advanced numerical algorithms for indirect evaluation of a selected body pose [14, 15].

IMU sensors are widely used in wearable electronics in order to estimate human body behavior in activities of daily living (ADL), orthopedics and rehabilitation, and they also help detect falls. Most commonly the IMU sensors are placed in the middle of the analyzed body segments. Basing on the kinematic data registered this way, the movement of the skeletal system can be simulated by a set of links connected together by joints with an adjusted degree of freedom (DOF) to reflect anatomical joints. Such kinematic models allow to analyze the motion of the human body as well as its individual segments, which can be treated as inverted pendulums. Such an approach was presented by Lin and Kulić, among others, and they have used wireless IMU sensors to estimate human leg posture and compared their results with the Motion Capture system [16]. IMU sensors were also used by Baldi *et al.* to estimate upper body pose to obtain similar, promising results [17]. Nowadays, a noticeable increase of interest in using IMU sensors for detecting falls can also be noticed. Such systems were already presented by Ruiz *et al.* or by Kim *et al.* [18, 19]. Even though they can be used to detect falls, by relying on a single IMU sensor, they do not provide information about kinematic parameters that, after appropriate processing, could reveal the cause of the fall. This suggests a

*e-mail: p.prochor@pb.edu.pl

Manuscript submitted 2023-04-06, revised 2023-07-01, initially accepted for publication 2023-11-25, published in February 2024.

certain need of designing a more complex system that would allow for better understanding of events occurring during human motion.

IMU sensor records are based on physical quantities measured by combinations of accelerometers (g – acceleration), gyroscopes (ω – angular velocity) as well as magnetometers (B – magnetic field), and only after combining these parameters it is possible to receive desired information about the position and orientation of the tested object. For this reason, appropriate data processing is required as every sensor suffers from errors during registration. Accelerometers' records are characterized by noise and are sensitive to linear acceleration. Amasay *et al.* proved this statement in their research during static and dynamic tests with accelerometers placed on a rotating vise [20]. In the case of gyroscopes' records, data are susceptible to low-frequency drift, which Feng *et al.* took into account during designing a new quaternion-based Kalman filter [21]. The last type of the above-listed sensors, i.e. magnetometers, is sensitive to hard and soft iron distortions. De Vries *et al.* presented the study for IMU sensors examination of influence of distortion of the earth magnetic field on measurements. According to their conclusions, requirements such as laboratory "mapping" or the use of a Kalman filter must be met to reduce magnetic disturbances [22].

These technical issues have a direct impact on data acquisition and their reliability. That is why applications of these sensors, among data fusion, require also implementation of properly selected filters. The most popular include the complementary filter [23] and the Kalman filter [24, 25], which can be used separately, combined or in appropriate sets. Correctly chosen parameters of these filters are decisive in establishing procedure, allowing to obtain results with desired accuracy and sensitivity. The crucial part of data processing is defining optimal calculation algorithms and in the case of filter usage – appropriately chosen parameters. Gui *et al.* used both complementary and Kalman filters to improve IMU's tilting measurements basing on 6-DOF and confirming their efficiency [26]. Yi *et al.* proposed their own complementary filter and compared its performance with others, such as the Kalman filter. IMU sensors were used and validation of an improved complementary filter was done during movement simulated with the usage of a 4-DOF test machine [27]. Ligorio *et al.* focused in their study on establishing a human body pose with the use of a tri-axial accelerometer and tri-axial-gyroscope. A wrist-worn IMU was tested during dynamic tasks and body pose was evaluated with the usage of a linear Kalman filter [28].

Above-described research as well as several other studies used different data processing methods in wearable electronics. As the most efficient data processing approach was never defined, certain questions can be asked: 1 – Can data processing algorithms ensure sufficient accuracy for estimating human body pose via wearable systems? 2 – How to process the IMU sensor data to obtain the most accurate information on the human body pose? Answers to these questions are crucial for designing appropriate equipment to e.g. detect and prevent falls or at least support persons with balance disorders. Therefore, the main purpose of the presented research was the evaluation of algorithms proposed by the authors to process the data obtained via an IMU sensor in order to estimate human body pose. Algorithms were evaluated in terms of accuracy and reliability with the use of parameters designated by the authors.

2. MATERIALS AND METHODS

2.1. Data acquisition

The test device collecting data was based on usage of IMU sensors (MPU6050 modules, IvenSense, San Jose, USA) which consist of a three-axis accelerometer and three-axis gyroscope. Seven of them have been wire-connected with an Arduino Due board based on a 32-bit ARM core microcontroller, and then programmed with Arduino Software (IDE). Communication of the modules was performed with an Inter-Integrated Circuit (I2C) bus, which allowed to collect data with specific timing. On the level of registers of sensors, sensitivity of accelerometers and gyroscopes was defined and ranges of measurement were set as $-16\ \mathrm{g} \div +16\ \mathrm{g}$ for accelerometers and $-2000^\circ/\mathrm{s} \div +2000^\circ/\mathrm{s}$ for gyroscopes. Threshold values were set on the basis of sensors' documentation as appropriate for the simulated type of movement. The device was powered by a USB cable from a portable battery or computer, in the first case recording data on a portable storage medium and in the second case simultaneously sending recorded data via serial port to a text file. Scheme of the test device, powered by a portable battery, is presented in Fig. 1a.

Collected and saved data included direct readings, such as: time based on microcontroller timer, accelerations along the X, Y, and Z axis of the sensor (Fig. 1b) and angular velocities around them, as well as those calculated by program parameters: components of quaternions calculated from accelerations as well

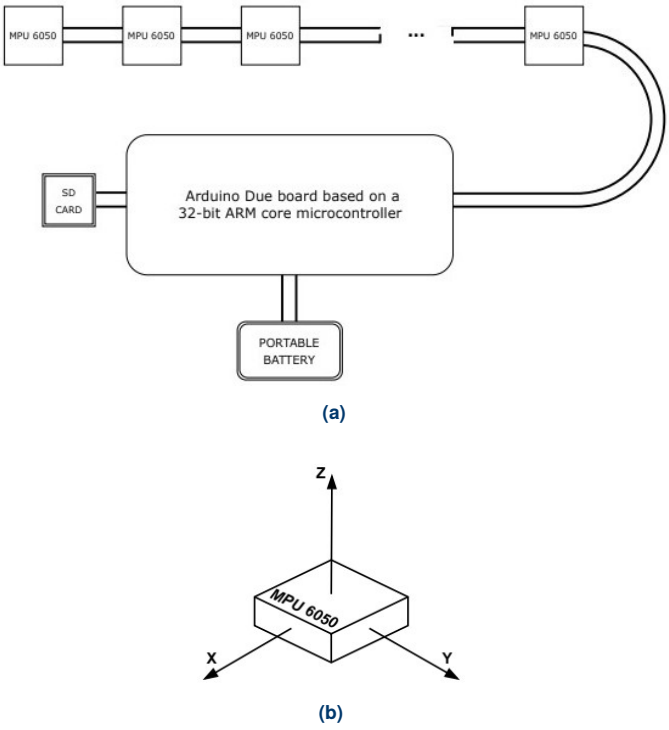

Fig. 1. (a) Scheme of the test device; (b) Axes of the sensor in module MPU 6050

as roll, pitch and yaw (RPY) angles (roll as tilt around X axis, pitch – around Y axis and yaw – around Z axis) calculated from readings of both accelerometers and gyroscopes.

Biodex System 4 PRO was used as a reference device, because of its ability to perform movement with set angular velocity and within an adaptable angular range. This allowed to obtain controlled and, most importantly, objective conditions, needed during the presented evaluation. Biodex System was set to move the attachment, which was placed on the dynamometer, without assistance (passive mode) – the attachment was moving rotationally, with the center of rotation in the dynamometer. The procedure was designed to test sensors in simulated human-like motion, and then tests were carried out for seven angular velocities: 10, 20, 30, 45, 60, 90 and 120°/s, every one of them in five angular movement ranges (AMR): from 0 to 30, 45, 60, 90 or 120°. Every test consisted of ten repetitions of pendulum movement (a single repetition was the movement away and towards) and was repeated 3 times with 5 seconds' break in between. To perform series of described tests, sensors were rigidly fixed to the attachment in three configurations – each enabling examination of the sensor in terms of movement around one of its axes (Fig. 1b), which can provide different results.

Considered configurations referred to the same movement of the attachment with sensors in different orientations. Configurations with orientation of the sensor were presented schematically in Fig. 2: A – orientation of sensors to record movement around Z axis; B – orientation of sensors to record movement around Y axis; C – orientation of sensors to record movement around X axis.

Finally, in the research 105 tests were carried out (movement around each of the three axes of the sensor multiplied by 7 tested angular velocities multiplied further by 5 angular movement ranges) and three repetitions were done in all cases. Additionally, in all trials 7 sensors were tested, as it was described above.

2.2. Data processing

For the research, four different data processing procedures for pose estimation were considered. Pose of the objects was analyzed as changing angular position during its movement. All procedures included different use (by order or in different set) of several variables, calculated on the basis of angular velocities and linear accelerations, such as: RPY angles, quaternions and angular position in general, with or without filtration (complementary and/or Kalman filter). Angular velocity and angular position of the attachment were analyzed and compared with the data recorded by a reference device. Data were analyzed depending on their type – angular velocity (ω) or angular position (α). Angular velocity was collected directly from the sensor component – gyroscope, that is why data were not modified for the sake of comparisons. In the case of angular position, as it is influenced by the pose of the moving object, it required a set of calculations.

Angular position was calculated on the basis of linear accelerations and angular velocities. To obtain RPY angles, roll and pitch were calculated from readings of the accelerometer according to formula (1) and (2) [29], and yaw was obtained from the gyroscope, calculating the angle for current time and for every next step summing previous values with the currently calculated ones (formula (3)):

$$\Phi = \arctan\left(\frac{A_Y}{\sqrt{A_X^2 + A_Z^2}}\right), \tag{1}$$

$$\Theta = \arctan\left(\frac{-A_X}{\sqrt{A_Y^2 + A_Z^2}}\right), \tag{2}$$

$$\Psi_n = \Psi_{n-1} + \frac{\mathrm{d}\omega}{\mathrm{d}t}, \tag{3}$$

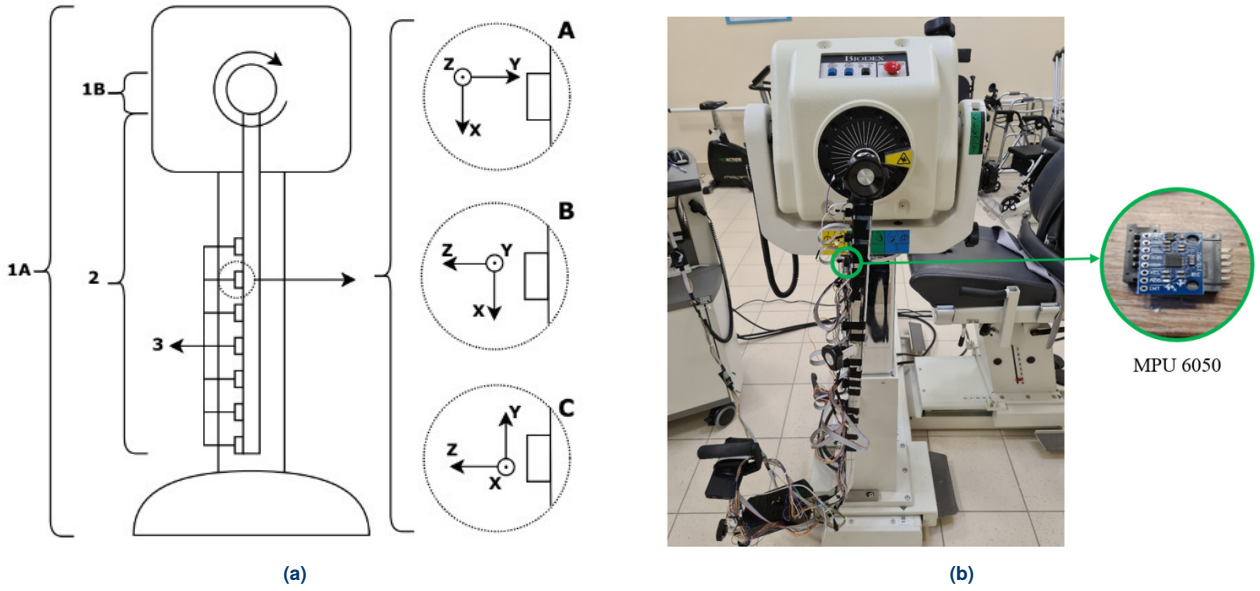

Fig. 2. Research setup: (a) scheme of configuration of axes of the sensors (1A – Biodex System, 1B – dynamometer, 2 – attachment, 3 – sensors); (b) Biodex System with sensors mounted according to configuration B

where: A_X – acceleration along X axis [m/s^2], A_Y – acceleration along Y axis [m/s^2], A_Z – acceleration along Z axis [m/s^2], Φ – roll (tilt around X axis) [°], Θ – pitch (tilt around Y axis) [°], ω – angular velocity [°/s], Ψ_{n-1} – yaw (tilt around Z axis) in previous moment of time [°], Ψ_n – yaw (tilt around Z axis) in present moment of time [°].

Formula (3) was applied to calculate roll and pitch as well, in order to fuse data between accelerometers and gyroscopes. Angles were then obtained by the use of a complementary filter, which is presented in formula (4):

$$\gamma = x \cdot \text{angle}_{\text{acc}} + (1-x) \cdot \text{angle}_{\text{gyro}}, \tag{4}$$

where: $\text{angle}_{\text{acc}}$ – angle calculated based on acceleration [°], $\text{angle}_{\text{gyro}}$ – angle calculated based on angular velocity [°], x – constant $\in \langle 0, 1 \rangle$, γ – angle calculated with the use of the complementary filter [°].

Quaternions, more specifically versors that are unit quaternions, were calculated strictly based on accelerations. This was done to provide information about body pose in the form of the vector with four elements. Quaternions represented by accelerations in the form of a vector are presented in (5) [30, 31]:

$$q_{\text{acc}} = \begin{cases} \left[\sqrt{\dfrac{A_Z+1}{2}} \quad -\dfrac{A_Y}{\sqrt{2\,(A_Z+1)}} \quad \dfrac{A_X}{\sqrt{2\,(A_Z+1)}} \quad 0 \right]^T \\ \qquad\qquad \text{if } A_Z \geq 0, \\ \left[-\dfrac{A_Y}{\sqrt{2\,(1-A_Z)}} \quad \sqrt{\dfrac{1-A_Z}{2}} \quad 0 \quad \dfrac{A_X}{\sqrt{2\,(1-A_Z)}} \right]^T \\ \qquad\qquad \text{if } A_Z < 0, \end{cases} \tag{5}$$

where: q_{acc} – quaternions calculated based on accelerations.

Quaternions have been converted into RPY angles and used in this study, because of the aforementioned fusion of angles obtained from accelerometers and gyroscopes – body pose represented by 8 quaternions cannot be included in the calculations of a complementary filter in its form used in the study. Conversion from quaternion to RPY angles was performed according to formulas (6), (7) and (8) [32]:

$$\Phi = \text{atan2}\left(2\,(q_2 q_3 - q_0 q_1), 2q_0^2 - 1 + 2q_3^2\right), \tag{6}$$

$$\Theta = -\arctan\left(\frac{2\,(q_1 q_3 - q_0 q_2)}{\sqrt{1-(2q_1 q_3 + 2q_0 q_2)^2}}\right), \tag{7}$$

$$\Psi = \text{atan2}\left(2\,(q_1 q_2 - q_0 q_3),\ 2q_0^2 - 1 + 2q_1^2\right), \tag{8}$$

where: atan2 – function which returns the value of arctan in the range from $-\pi$ to π [rad]; q_0, q_1, q_2, q_3 – elements of the quaternion's versor.

In their transformed form, angles from quaternions were fused with those from gyroscopes by a complementary filter. The use of values from both types of sensors minimized the influence of their errors on results.

Kalman filters were considered another method for minimizing the influence of errors from sensors on the results obtained. Establishing the state extrapolation equation was the first step in designing a Kalman filter for this case of calculating an angular position (formula (9)):

$$x_k = Fx_{k-1} + Gu = \begin{bmatrix} 1 & 0 & -dt \\ 0 & 0 & -1 \\ 0 & 0 & 1 \end{bmatrix} \begin{bmatrix} \theta \\ \omega \\ g_{\text{bias}} \end{bmatrix}_{k-1} + \begin{bmatrix} dt \\ 1 \\ 0 \end{bmatrix} u, \tag{9}$$

where: F – state transition matrix, G – control matrix, x – state vector, θ – angle [°], ω – angular velocity [°/s], g_{bias} – gyroscope's bias [°/s], u – control variable.

Defining matrices, crucial for the prediction and update parts of the Kalman filter, was the second part of the operation. The Kalman filter was used in two of the algorithms, which served for obtaining an angular position from the recording of the sensors. Finally, there were 4 methods of data processing (Table 1) and for each method statistical measures were calculated and compared with the angular position obtained from Biodex System.

This comparison led to selecting a data processing algorithm characterized by the best accuracy and relevance (with the lowest differences between the values obtained from sensors and the reference device).

The difference between angular velocity values as well as Spearman's correlation coefficients between angular velocity in time, registered by use of the tested and reference systems, were analyzed, to evaluate accuracy of angular velocity registration with the use of the tested system. In the case of differences between angular velocity values, firstly absolute values from every test were summed and divided by the number of samples in the test (schematic representation in Fig. 3 and (10)). Calculation of both stable maximum values and increasing/decreasing values was intentional in order to compare results from sensors and Biodex System. Parameters for each filter (Kalman and/or complementary) were individually set in each algorithm in order to obtain the best values of Spearman's correlation coefficients for each selected algorithm (A1–A4), among others. Such a procedure was performed in order to objectively compare the data processing methods being evaluated.

$$\overline{\omega} = \frac{\sum_{i=1}^{s} |\omega_i|}{s}, \tag{10}$$

where: $|\omega_i|$ – absolute value of angular velocity [°/s], $\overline{\omega}$ – mean value of angular velocity for a single test [°/s], s – number of samples.

Mean values of angular velocity were calculated for values registered by the IMU sensors system, separately for each sensor for all 315 test repetitions. The obtained values were then averaged for three repetitions of each test ($\overline{\omega}_S$). Averaging between repetitions was also applied to the angular velocity generated by the reference system ($\overline{\omega}_B$). For evaluation accuracy of the tested system, the difference between averaged values of angular velocity obtained from individual sensors and Biodex System were

Table 1
Classification of signal quality as a function of its power

No.	Used sensors	Description
A1	accelerometer	accelerations → quaternions → final angles
A2	accelerometer + gyroscope	accelerations → quaternions → angles; angular velocities → integration → angles; angles → complementary filter → final angles
A3	accelerometer + gyroscope	accelerations → quaternions → angles → Kalman filter → final angles; angular velocities → Kalman filter
A4	accelerometer + gyroscope	accelerations → quaternions → angles; angular velocities → integration → angles; angles → complementary filter → angles → Kalman filter → final angles; angular velocities → Kalman filter

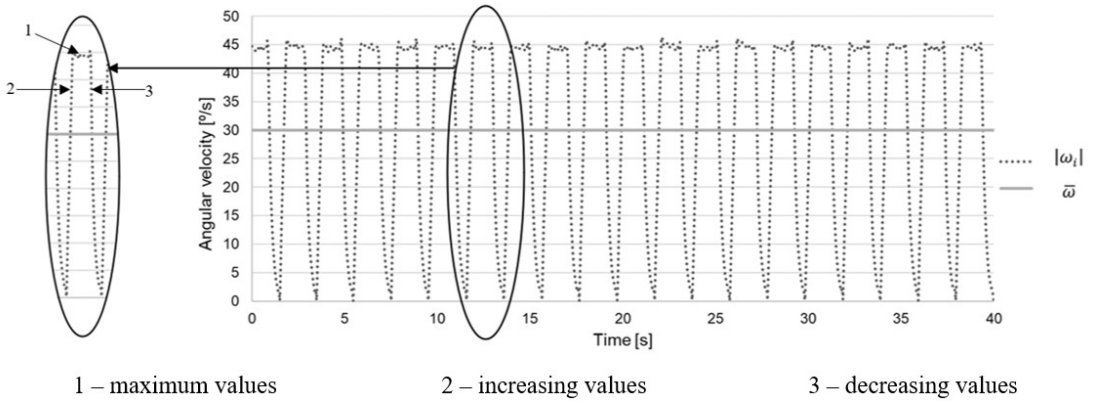

Fig. 3. Changes in absolute angular velocity with its mean representation for a single test: 1 – maximum values; 2 – increasing values; 3 – decreasing values

determined for each test using the formulas below:

$$\Delta_\omega = \overline{\omega}_B - \overline{\omega}_S\,, \tag{11}$$

$$\varepsilon_\omega = \frac{\overline{\omega}_B - \overline{\omega}_S}{\overline{\omega}_B} \cdot 100\%, \tag{12}$$

where: Δ_ω – difference between angular velocity obtained from individual sensors of the tested system and reference (Biodex) system [°/s], ε_ω – relative difference between angular velocity obtained from individual sensors of the tested system and reference (Biodex) system [%].

Next, these parameters were averaged for all analyzed values of angular velocities and angular movement ranges (AMR), separately for every axis of movement (X, Y and Z axis):

$$\overline{\Delta_\omega} = \frac{\sum_{i=1}^{n} (\Delta_{\omega i})}{n}\,, \tag{13}$$

$$\overline{\varepsilon_\omega} = \frac{\sum_{i=1}^{n} (\varepsilon_{\omega i})}{n}\,, \tag{14}$$

where: $\overline{\Delta_\omega}$ – difference between angular velocity obtained from individual sensors of the tested system and reference (Biodex) system averaged for all angular velocities and AMR [°/s],

$\overline{\varepsilon_\omega}$ – relative difference between angular velocity obtained from individual sensors of the tested system and reference (Biodex) system averaged for all angular velocities and AMR [%], $n = 35$ (number of tested angular velocity multiplied by the number of AMR).

Parameters presented above were calculated separately for each of the seven IMU sensors and next averaged:

$$\mathrm{AVG}_{\overline{\Delta_\omega}} = \frac{\sum_{i=1}^{n_s} \left(\overline{\Delta_{\omega_l}}\right)}{n_s}, \tag{15}$$

$$\mathrm{AVG}_{\overline{\varepsilon_\omega}} = \frac{\sum_{i=1}^{n_s} \left(\overline{\varepsilon_{\omega_l}}\right)}{n_s}. \tag{16}$$

Spearman's correlation coefficients between values of angular velocity in time, gathered from individual sensors and Biodex System (C_{SB_ω}), respectively for every test, were calculated and averaged for three repetitions ($\overline{C_{\mathrm{SB}_\omega}}$) made for each test as well. These mean values were next averaged for all analyzed values of angular velocities and AMR, separately for every axis of movement (X, Y and Z axis):

$$\mathrm{Mean}_{\overline{C_{\mathrm{SB}_\omega}}} = \frac{\sum_{i=1}^{n} \left(\overline{C_{\mathrm{SB}_{\omega_i}}}\right)}{n}, \tag{17}$$

where: $\mathrm{Mean}_{\overline{C_{\mathrm{SB}_\omega}}}$ – Spearman's correlation coefficients between values of angular velocity over time from tested and reference (Biodex) systems averaged for all angular velocities and AMR.

Averaged values for all angular velocities and AMR Spearman's correlation coefficients were calculated separately for each of the seven IMU sensors and then averaged:

$$\mathrm{AVG}_{C_{\mathrm{SB}_\omega}} = \frac{\sum_{i=1}^{n_s} \left(\mathrm{Mean}_{\overline{C_{\mathrm{SB}_{\omega_l}}}}\right)}{n_s}, \tag{18}$$

where: $\mathrm{AVG}_{C_{\mathrm{SB}_\omega}}$ – averaged for all IMU sensors Spearman's correlation coefficients between values of angular velocity over time from tested and reference (Biodex) systems.

Additionally, for evaluation of the accuracy of angular position estimation with the use of particular algorithms (Table 1), three statistical parameters were used: relative error of means (REM), error of Spearman's correlation coefficient (SCC) and relative error of extreme values (REE). REM and SCC were also used for additional angular velocity evaluation.

Mean values of angular position in the single test were calculated in a manner similar to the one described earlier for angular velocity (Fig. 4, formula (10)) and averaged between three repetitions of the test, using data taken from individual sensors and obtained with the use of particular algorithms $\overline{\alpha}_S$ as well as the reference system $\overline{\alpha}_B$. Relative difference between measurements from the tested and reference system was calculated as follows:

$$\varepsilon_\alpha = \frac{\overline{\alpha}_B - \overline{\alpha}_S}{\overline{\alpha}_B} \cdot 100\%, \tag{19}$$

where: ε_α – relative difference between angular position obtained from individual sensors of the tested system and reference (Biodex) system [%].

Averaged extreme values of angular position for 10 pendulum movements in a single test (Fig. 4) were calculated and next, again averaged between three repetitions of particular tests ($\overline{\alpha_{\mathrm{MAX}}}$).

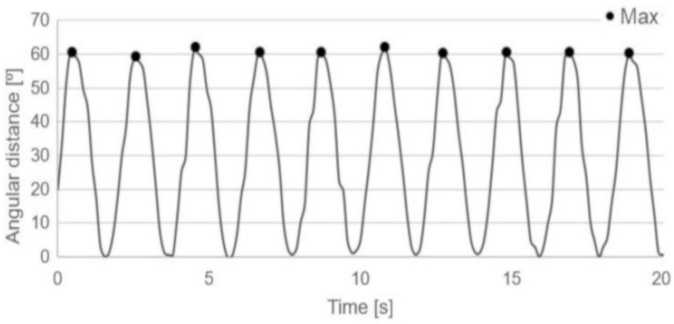

Fig. 4. Schematic representation of extreme values of angular position of every 10 pendulum movement in a single test

Averaged values described above were used to calculate relative difference between measurements of extreme values of angular position from the tested and reference systems, basing on the following formula:

$$\varepsilon_{\alpha_{\mathrm{MAX}}} = \frac{\overline{\alpha_{\mathrm{MAX}_B}} - \overline{\alpha_{\mathrm{MAX}_S}}}{\overline{\alpha_{\mathrm{MAX}_B}}} \cdot 100\%, \tag{20}$$

where: $\varepsilon_{\alpha_{\mathrm{MAX}}}$ – relative difference between extreme angular position obtained from individual sensors of the tested system and reference (Biodex) system [%].

The parameter calculated using (12) and (19) was calculated for all angular velocities and all AMR, separately for each of the seven IMU sensors, and next averaged:

$$\mathrm{REM}_\omega = \frac{\sum_{i=1}^{n_s} \left(\varepsilon_{\omega_i}\right)}{n_s}, \tag{21}$$

$$\mathrm{REM}_\alpha = \frac{\sum_{i=1}^{n_s} \left(\varepsilon_{\alpha_i}\right)}{n_s}, \tag{22}$$

where: REM_ω – relative error of means of angular velocity calculated separately for each of 105 tests (movement around each of the three axes of the sensor multiplied by 7 tested angular velocities multiplied by 5 angular movement ranges) [%], REM_α – relative error of means of angular position calculated separately for each of the four algorithms and each of 105 tests (movement around each of the three axes of the sensor multiplied by 7 tested angular velocities multiplied further by 5 angular movement ranges) [%].

In the case of angular position estimation, relative error of extreme values (REE) was also calculated using (23):

$$\mathrm{REE} = \frac{\sum_{i=1}^{n_s} \left(\varepsilon_{\alpha \mathrm{MAX}_i} \right)}{n_S}, \tag{23}$$

where: REE – relative error of extreme values of angular position calculated separately for each of the four algorithms and each of 105 tests (movement around each of the three axes of the sensor multiplied by 7 tested angular velocities multiplied further by 5 angular movement ranges) [%].

Spearman's correlation coefficients, described earlier for angular velocities ((17) and (18)) were averaged firstly for all tested angular velocity and AMR, and next averaged for all sensors. However, for analysis of the influence of particular angular velocity or AMR, another methods of analysis was proposed. Spearman's correlation coefficients, comparing data from tested and reference systems, averaged between three repetitions of every test, were calculated both for angular velocity ($\overline{C_{\mathrm{SB}_{\omega_i}}}$) and angular position ($\overline{C_{\mathrm{SB}_{\alpha_i}}}$), separately for particular values of the tested angular velocities and particular AMR. Parameters presented above were calculated separately for each of the seven IMU sensors and next averaged:

$$\mathrm{SCC}_\omega = \frac{\sum_{i=1}^{n_s} \left(\overline{C_{\mathrm{SB}_{\omega_i}}} \right)}{n_S}, \tag{24}$$

$$\mathrm{SCC}_\alpha = \frac{\sum_{i=1}^{n_s} \left(\overline{C_{\mathrm{SB}_{\alpha_i}}} \right)}{n_S}, \tag{25}$$

where: SCC_ω – Spearman's correlation coefficient between angular velocity over time from the tested and reference (Biodex) systems, averaged for all sensors, SCC_α – Spearman's correlation coefficient between angular position over time from the tested and reference (Biodex) systems, averaged for all sensors.

3. RESULTS

3.1. Angular velocity

Angular velocity of the moving object was obtained using both tested and reference systems. The differences between their indications were evaluated using statistical measures described earlier ((15) and (16)). Averaged values with standard deviation ($\mathrm{AVG}_{\overline{\Delta_\omega}} \pm \mathrm{STD}_{\overline{\Delta_\omega}} \mathrm{AVG}_{\overline{\varepsilon_\omega}} \pm \mathrm{STD}_{\overline{\varepsilon_\omega}}$) and dispersion between minimum and maximum values ($\mathrm{DIS}_{\overline{\Delta_\omega}} \mathrm{DIS}_{\overline{\varepsilon_\omega}}$) for these differences were compiled in Table 2.

Results of Spearman's correlation coefficient between values of angular velocity over time from tested and reference (Biodex) systems (formula (18)) – averaged values with standard deviation ($\mathrm{AVG}_{C_{\mathrm{SB}_\omega}} \pm \mathrm{STD}_{C_{\mathrm{SB}_\omega}}$) and dispersion between minimum and maximum values ($\mathrm{DIS}_{C_{\mathrm{SB}_\omega}}$) were presented in Table 3.

Tables 2 and 3 include results averaged for all angular velocities, angular movement ranges (AMR) and all sensors. Parameters REM_ω (equation (21)) and SCC_ω (equation (24)) were averaged only for all sensors and considered with a distinction of axes of movement and of angular velocities. As a result, box-whiskers plots were created: REM_ω in Fig. 5, SCC_ω in Fig. 6.

Table 2
Statistical measures describing differences between angular velocity measured by tested IMU system and reference system

	X axis	*Y* axis	*Z* axis
$\mathrm{AVG}_{\overline{\Delta_\omega}} \pm \mathrm{STD}_{\overline{\Delta_\omega}}$ [°/s]	0.82 ± 0.39	1.05 ± 0.65	0.55 ± 0.33
$\mathrm{DIS}_{\overline{\Delta_\omega}}$ [°/s]	3.20	4.40	2.27
$\mathrm{AVG}_{\overline{\varepsilon_\omega}} \pm \mathrm{STD}_{\overline{\varepsilon_\omega}}$ [%]	2.76 ± 1.27	3.11 ± 1.87	1.76 ± 1.02
$\mathrm{DIS}_{\overline{\varepsilon_\omega}}$ [%]	4.96	7.08	4.11

Table 3
Statistical measures describing Spearman's correlation coefficient between values of angular velocity in time from tested and reference (Biodex) systems

	X axis	*Y* axis	*Z* axis
$\mathrm{AVG}_{C_{\mathrm{SB}_\omega}} \pm \mathrm{STD}_{C_{\mathrm{SB}_\omega}}$	0.89 ± 0.01	0.88 ± 0.01	0.89 ± 0.01
$\mathrm{DIS}_{C_{\mathrm{SB}_\omega}}$	0.53	0.41	0.36

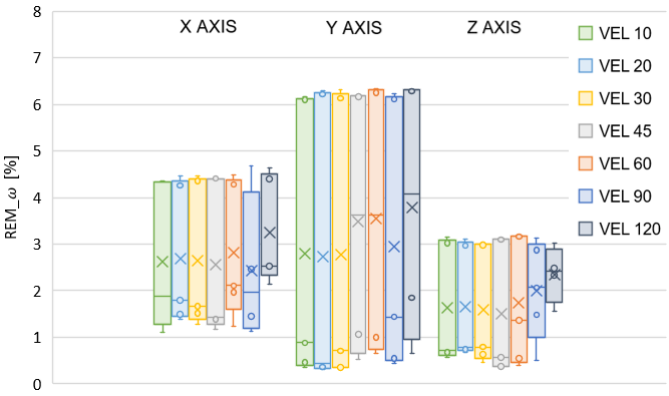

Fig. 5. REM_ω for different values of angular velocity for movement around *X*, *Y* and *Z* axes

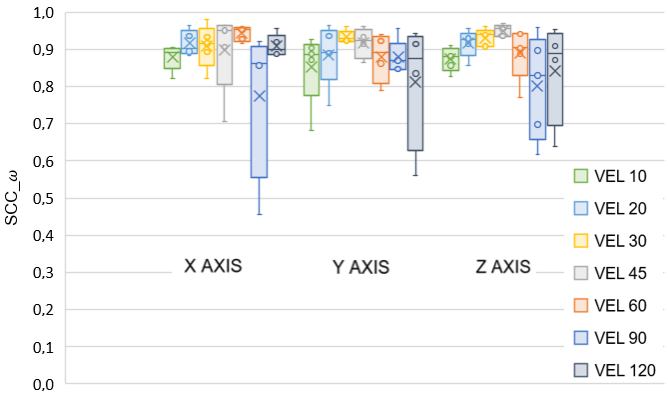

Fig. 6. SCC_ω for different values of angular velocity for movement around *X*, *Y* and *Z* axes

Dispersions visible on the plots resulted from the fact that for every direction of movement (around the X, Y and Z axis) and every value of angular velocity (10, 20, 30, 45, 60, 90, 120°/s), there were five values, both in the case of REM_ω and SCC_ω, obtained for every of five AMR (30, 45, 60, 90 and 120°).

3.2. Pose estimation

Pose estimation of the moving objects was analyzed as changes in angular position during movement around every axis (X, Y and Z). REM_α, REE and SCC_α of angular position were calculated as was described in (22), (23) and (25). Results for each AMR and for every algorithm were presented in Fig. 7 (REM_α), Fig. 8 (SCC_α) and Fig. 9 (REE), separately for movement around the X, Y and Z axis. The dispersions visible on plots resulted

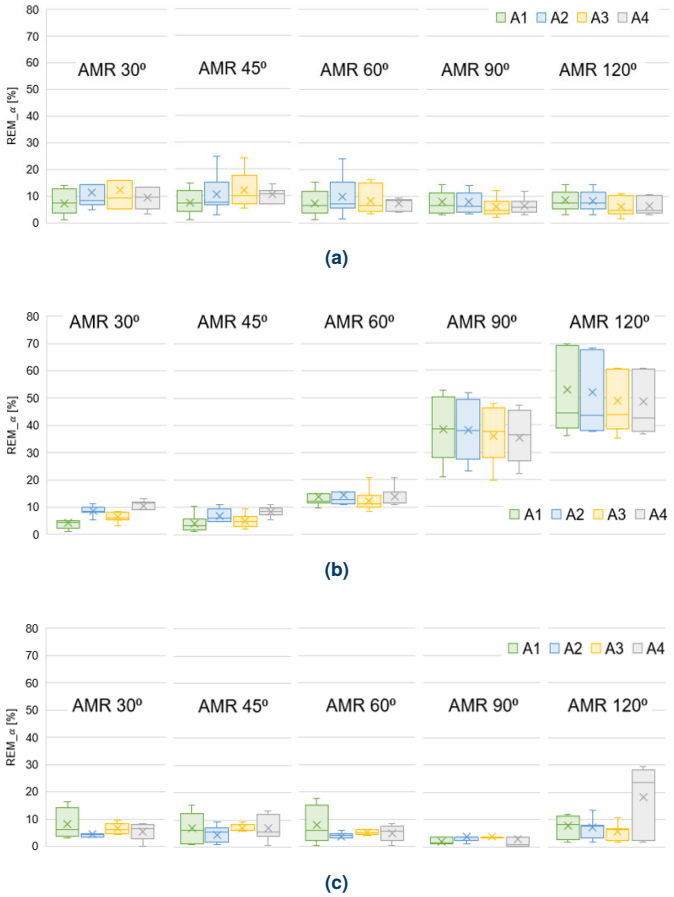

Fig. 7. REM_α for every algorithm (A1, A2, A3, A4 – Table 1) and for all AMR in movement around: (a) X axis; (b) Y axis; (c) Z axis

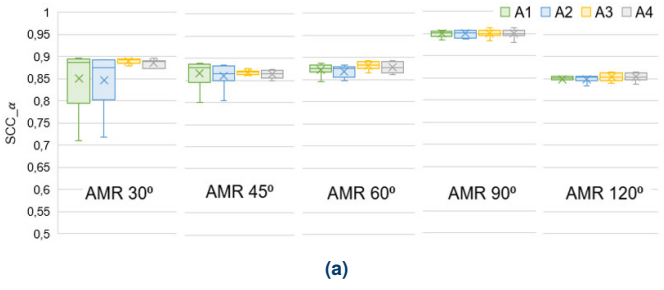

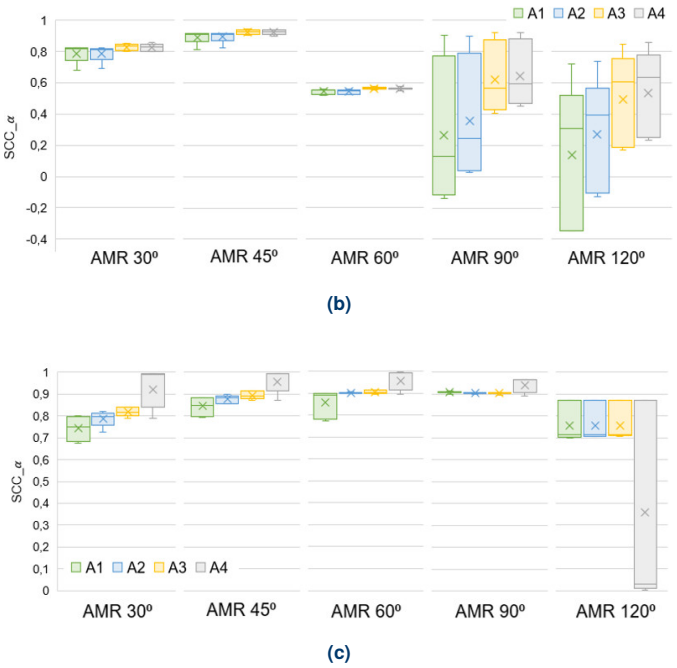

Fig. 8. REM_α for every algorithm (A1, A2, A3, A4 – Table 1) and for all AMR in movement around: (a) X axis; (b) Y axis; (c) Z axis

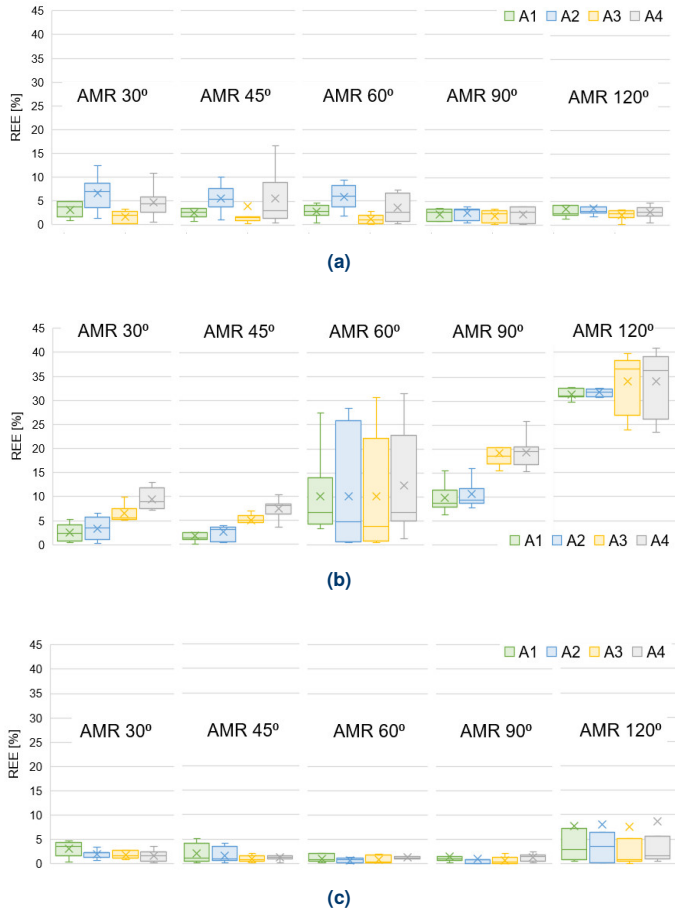

Fig. 9. REE for every algorithm (A1, A2, A3, A4 – Table 1) and for all AMR in movement around: (a) X axis; (b) Y axis; (c) Z axis

from the fact that for every value of AMR (30, 45, 60, 90 and 120°), for each analyzed algorithm, there were seven values of particular parameters obtained for different angular velocities (10, 20, 30, 45, 60, 90 and 120°/s).

4. DISCUSSION

The results obtained for angular velocity were analyzed separately for every axis. Maximum averaged difference between angular velocity from tested and reference systems stood at 1.05°/s for absolute values and at 3.11% for relative values obtained for movement around the *Y* axis, which means the worst accuracy of these type of data. Registration around the *Z* axis indicated the best results – averaged difference of 0.55°/s for absolute values and 1.76% for relative values. Additionally, analyzing the relative error of means for every angular velocity (REM_ω), the best accuracy was obtained for registering data for the *Z* axis (from 0.36% to 3.19%), while the worst for the *Y* axis (from 0.31% to 6.33%). What is more, no dependency between the accuracy and the value of angular velocity was noted. Differences in values of the error of Spearman's correlation coefficient (SCC_ω) were noticeable – the lowest values of SCC_ω occurred for angular velocity equal to 90°/s (0.45) and 120°/s (0.56) for all the axes. Due to the fact that SCC_ω is a parameter used to compare compliance of time waveforms, it is sensitive to differences such as phase shifts, which appeared for higher velocities, especially when they are combined with small angular movement ranges (AMR). Observed differences between the values might be caused by inertia in the sensors used, which was already observed and confirmed by Shaeffer *et al.* [33].

The results obtained in the case of an angular position were also analyzed separately for every axis. REM_α for all AMR, suggests the necessity of individual choice of the data processing algorithm, depending on the axis being analyzed. Average value and dispersion of the box-whiskers plots were taken into consideration in the decision-making process of the algorithm with the best accuracy. For data recorded for the *X* axis, the best results were obtained by calculating angle values on the basis of accelerations with the use of quaternions (algorithm A1). In this case, average REM_α was equal to 7.55%. This confirmed earlier literature reports about the usefulness of quaternions in estimating positions in three-dimensional space [34]. For data recorded for the *Y* axis, according to the presented distribution (Fig. 7b), the best results were obtained by calculating angle values directly from accelerations with the use of quaternions (algorithm A1) or from accelerations while using quaternions and applying the Kalman filter (algorithm A3). In the first and second cases, average REM_α was equal to 22.78% and 21.7%, respectively, which was considered too high. Both algorithms, which used the data from gyroscopes, delivered worse results, which is directly correlated with the highest inaccuracies of angular velocity registration in the case of movement around the *Y* axis. What is more, all algorithms failed when for movement around the *Y* axis, AMR was equal or greater than 90°, which results from Euler angles limitations. Failure is caused by the necessity of changing quaternions into Euler angles, when a basic form of complementary filter is used. This suggests that orientation of an IMU based system should prevent the *Y* axis of sensors from overlapping with the direction of the largest AMR, if transformation of quaternions into Euler angles is performed. However, Valenti *et al.* performed fusion that was similar in purpose, using data directly in the form of quaternions and proposing a novel quaternion based complementary filter, allowing to avoid Euler angles limitations [30]. After exclusion of data registered for AMR equal or greater than 90°, algorithm A1 and algorithm A3 still provided the highest accuracy, and average REM_α was respectively lowered to 7.47% and 7.86%. In the case of data recorded for the *Z* axis, the best results were obtained by calculating angles from accelerations with the use of quaternions and angular velocity through integration and then application of a complementary filter (algorithm A2). In that case the average REM_α was equal to 4.78%. This confirmed earlier literature reports that sensor data fusion and proper choice of filter parameters can increase reliability and accuracy of results. Guo *et al.* confirmed this observation in their research with the use of a Kalman filter and information fusion, which allowed to improve the detection accuracy of the gyroscope [35]. Although registration of angular velocity around the *Z* axis ensures high accuracy, the use of additional filters is not necessary and could generate higher computational cost. Similar conclusions were presented by Gui *et al.*, who stated that results from both filter types (complementary and Kalman) can work effectively. However, because of computational complexity of the Kalman filter, it is not always a suggested tool to be used [26].

Except for REM_α, distribution of SCC_α was taken into consideration as well. As SCC_α depends on the compliance of time waveforms, the SCC_α results suggested a different approach in selecting an appropriate data processing algorithm. The best results, for every axis, were obtained for angles calculated from quaternions and filtered with the use of a Kalman filter (algorithm A3). Average SCC_α was equal to 0.89 for results in the case of the *X* axis, 0.77 for the *Y* axis and 0.86 for the *Z* axis. The accuracy of the algorithm in terms of SCC_α highly depends on the shape of the waveform. As the Kalman filter allows to smooth curves obtained on the basis of data from sensors, by eliminating noises characteristic for accelerometer recordings, it led to obtaining high accuracy for the algorithm being described. This effect is correlated with the Kalman filter parameters, which influence its dynamics characteristic and have the impact of inertia in estimated signals [36]. Finally, it must be stated that extreme values of the angular position reached by a moving object (Fig. 4) have a special meaning for pose evaluation. Therefore, its relative errors of extreme values (REE) of angular position were considered most important for the examination of human body movement. Calculated values of REE for all AMR for the *X* axis suggested that while calculating angles from accelerations with the use of quaternions and the Kalman filter (algorithm A3), it allows to obtain the best results (average REE was equal to 2.15%). However, other algorithms also ensured similar results – maximum of average REE was equal to 4.81% (algorithm A2). The results obtained for the *Y* axis suggested to calculate angles directly from accelerations with the use of quaternions (algorithm A1) – in that

case average REE was equal to 11.1% or 4.81% after excluding results for AMR equal or greater than 90°. For the Z axis, the best results were obtained again by calculating angles from accelerations with the use of quaternions and the Kalman filter (algorithm A3) – average REE was equal to 2.38%. In the case of the Z axis, taking into consideration the values of REE, every algorithm would be acceptable for application, because the maximum value of averaged REE was relatively small and equal to 3.04% (algorithm A1).

The results obtained after calculating REE show relatively the best accuracy independently of the type of algorithm used for two of the three axes (X and Z axis). This suggests that the use of any of the proposed algorithms would ensure a proper performance of the system for these axes during the monitoring of body pose, if significant changes of body position are taken into consideration. This can be crucial in the case of human locomotion to identify threatening situations.

Analysis of angular position with the use of REM_α, SCC_α and REE provided information about the distribution of obtained values, time waveform and extreme values. Efficiency of evaluated algorithms depended on the above-described parameters.

Table 4 presents acceptable algorithms, which were chosen on the basis of all parameters (REM_α, SCC_α, REE) for every axis, while Table 5 presents the most efficient ones. Algorithms were considered as acceptable when:

- REM_α values were lower than 10%;
- SCC_α values were higher than 0.7 (strong dependence) [37];
- REE values were lower than 5%.

Table 4
Algorithms classified as acceptable for movement around particular axis

	Algorithm A1	Algorithm A2	Algorithm A3	Algorithm A4
REM_α:				
X	+	+	+	+
Y	+		+	
Z	+	+	+	+
SCC_α:				
X	+	+	+	+
Y	+	+	+	+
Z	+	+	+	+
REE:				
X	+	+	+	+
Y	+			
Z	+	+	+	+
SUM	**9**	**7**	**8**	**7**

An algorithm was classified as the most efficient one when the smallest values in the case of REM?? and REE and the highest in the case of $\text{SCC}_{??}$ were obtained. Ranking parameters ($\text{REM}_\alpha < 10\%$ and $\text{REE} < 5\%$) resulted from their aforementioned characteristic. In the case of REM_α, both steady maximum and increasing/decreasing values were taken into consideration for comparison, which made this parameter less stable. REE was correlated only with the highest changes of position and the set of values placed in a specific, extreme range of registered data, stabilizing this parameter.

Table 5
The most efficient algorithms for movement around particular axis

	Algorithm A1	Algorithm A2	Algorithm A3	Algorithm A4
REM_α:				
X	+			
Y	+			
Z		+		
SCC_α:				
X			+	
Y			+	
Z			+	
REE:				
X			+	
Y	+			
Z			+	
SUM	**3**	**1**	**5**	**0**

According to acceptable (Table 4) and the most efficient (Table 5) algorithms:

1) in the first case:
   - two out of the four algorithms (algorithm A2 and A4) were acceptable 7 out of 9 times;
   - algorithm A3 was acceptable 8 out of 9 times;
   - algorithm A1 was acceptable 9 out of 9 times.
2) in the second case:
   - algorithm A4 was the most efficient 0 out of 9 times;
   - algorithm A2 was the most efficient 1 out of 9 times;
   - algorithm A1 was the most efficient 3 out of 9 times;
   - algorithm A3 was the most efficient 5 out of 9 times.

Results in Table 4 allowed to state that in terms of acceptability, all algorithms allowed to obtain satisfying results. While taking into consideration the results in Table 5, it is possible to indicate algorithm A3 as the most efficient one.

Registration of kinematic parameters was performed for certain values of angular velocity and angular position, which was correlated with human locomotion. However, it is possible that directly registered angular velocity and calculated angular position would have presented different results during higher or lower angular velocity. For this reason, for further evaluations, the tested system and proposed algorithms should have been used in multi-planed and dynamic movement – with simultaneous changes of body pose around every axis.

As shown in the results, establishing an algorithm which presents properly registered values of angular position for every axis during AMR equal or greater that 90° was out of reach with the proposed method, which resulted from physical and mathematical principles of sensors operations. An algorithm calculating angular position only based on the gyroscope readings would be resistant to limitations, but because of the generated drift, which occurs during integration of registered angular velocity into angular position, it was not included in the research presented herein. Moreover, during calculations of the complementary filter, values of angular position obtained from angular velocity were set as having lower influence on the results and were mostly used for smoothing rather than correcting final results.

Change of sensitivity through hardware calibration and more precise programmed calibration will be considered in future work over the system with IMU sensors, in order to attempt to avoid the negative impact of drift and, with the use of the angular position calculated from the gyroscope, overcome the limitations of Euler angles.

Obtained results can be directly used to process the data in mechatronic devices with systems for i.e. fall detections. However, appropriate placement of sensors is crucial for obtaining viable kinematic parameters. In Fig. 10a, we have suggested a positioning of sensors to monitor the human body pose, that is visualized in Fig. 10b directly on human body. Simplified version of the system in the form of a flexible vest, allowing to monitor body falls, was presented in Fig. 10c. All suggestions and designs are a matter of future studies.

Suggested placement of sensors finds justification in the models already presented and validated in the literature [38, 39]. An appropriate model used to create a mechatronic device consisting of inter alia IMU sensors with an implemented algorithm to efficiently process kinematic data can allow to e.g. monitor falls of the elderly during ADL. This can lead to obtaining data that are crucial for diagnosis as well as designing individual treatment to increase the quality of life.

5. CONCLUSIONS

According to the results obtained, the answers to the questions defined in the introduction are the following: 1 – Wearable systems can estimate human body pose with sufficient accuracy while using appropriate data processing algorithms; 2 – From all analyzed algorithms, the one calculating angles based on acceleration-derived quaternions and with implementation of the Kalman filter was classified as the most efficient. In the situation of ranking relative error of means (REM_α) as the most important and only parameter taken into consideration during evaluation, it would be advisable to omit Kalman filter implementation and to consider the angles from quaternions calculated on the basis of acceleration as sufficiently accurate. However selection of an appropriate method should be made considering calibration, data type and filtration. While designing a wearable system, there is a necessity of conducting an attempt to adjust the data processing method. It is crucial among others in systems for detecting and preventing falls or any other wearable device that is designated to support humans in daily activity.

Evaluating pendulum movement might be considered as oversimplification when conducting at attempt to estimate the usefulness of selected algorithms in data processing of real human motion. However, the differences obtained and presented within the manuscript have a direct impact on the performance of the algorithms being considered, allowing to conduct a statement of increased quality of selected data processing methods over different ones.

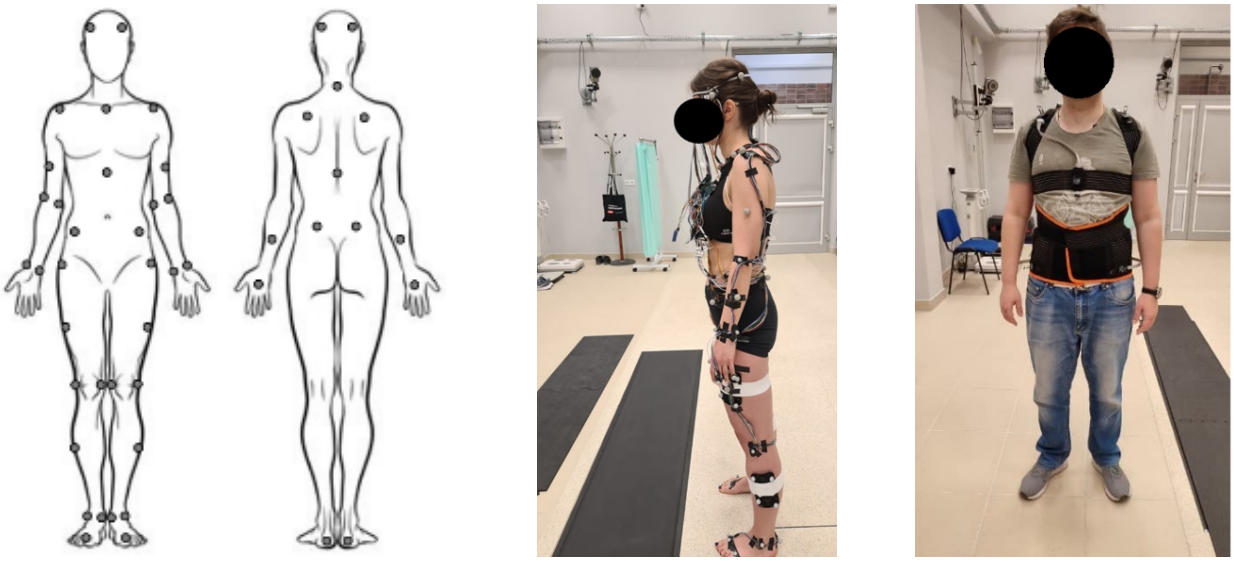

(a) (b) (c)

Fig. 10. Suggested sensors setup on human body: (a) sensors positioning, (b) direct placement of sensors on human body, (c) a prototype of the flexible vest for monitoring body falls – sensors on limbs were neglected for simplification purposes in initial version of the system (more sensors can be added in future studies)

Even though the obtained results directly present the influence of selected factors on the obtained data, it is important to remember that there are several different factors that have a significant impact on the accuracy of the results while using sensors in wearable robotics. The optimized number of sensors used to record the data or their symmetrical orientation can be distinguished among them. However, the research was designed to reduce the impact of non-analyzed factors and focus only on the data processing issue. Nevertheless, the evaluation of the influence of the other factors remains the goal for future studies.

ACKNOWLEDGEMENTS

This research was funded by the National Centre for Research and Development, as a part of the governmental "Accessibility Plus" program competition entitled "Things are for people". Project: "Mechatronic device to assist in maintaining balance during locomotion with function of recording gait kinematic parameters", contract No. Rzeczy są dla ludzi/0009/2020. Funding was also provided by the Polish Ministry of Science and Higher Education, project number WI/WM-IIB/6/2021.

REFERENCES

[1] K. Lee and W.A. Tang, "A Fully Wireless Wearable Motion Tracking System with 3D Human Model for Gait Analysis," *Sensors*, vol. 21, no. 12, p. 4051, 2021, doi: 10.3390/s21124051.

[2] A. Blanco Ortega *et al.* "Biomechanics of the Upper Limbs: A Review in the Sports Combat Ambit Highlighting Wearable Sensors," *Sensors*, vol. 22, no. 13, p. 4905, 2022, doi: 10.3390/s22134905.

[3] Y. Jiang, P. Malliaras, B. Chen, and D. Kulić, "Real-time forecasting of exercise-induced fatigue from wearable sensors," *Comput. Biol. Med.*, vol. 148, p. 105905, 2022, doi: 10.1016/j.compbiomed.2022.105905.

[4] R. Argent, P. Slevin, A. Bevilacqua, M. Neligan, A. Daly, and B. Caulfield, "Clinician perceptions of a prototype wearable exercise biofeedback system for orthopaedic rehabilitation: a qualitative exploration," *BMJ Open*, vol. 8, no. 10, p. e026326, 2018, doi: 10.1136/bmjopen-2018-026326.

[5] M. Ollenschläger *et al.*, "Wearable gait analysis systems: ready to be used by medical practitioners in geriatric wards?," *Eur. Geriatr. Med.*, vol. 13, no. 4, pp. 817–824, 2022, doi: 10.1007/s41999-022-00629-1.

[6] I.M. Pires, F. Hussain, G. Marques, and N.M. Garcia, "Comparison of machine learning techniques for the identification of human activities from inertial sensors available in a mobile device after the application of data imputation techniques," *Comput. Biol. Med.*, vol. 135, p. 104638, 2021, doi: 10.1016/j.compbiomed.2021.104638.

[7] Y. Guo *et al.*, "High-accuracy wearable detection of freezing of gait in Parkinson's disease based on pseudo-multimodal features," *Comput. Biol. Med.*, vol. 146, p. 105629, 2022, doi: 10.1016/j.compbiomed.2022.105629.

[8] W. Xu, Y. Zheng, C.H. Chu, L. Cheng, and J. Kim, "Applying deep learning technology for automatic fall detection using mobile sensors," *Biomed. Signal. Proces.*, vol. 72 (part B), p. 103355, 2022, doi: 10.1016/j.bspc.2021.103355.

[9] F. Ryser, S. Hanassab, O. Lambercy, E. Werth, and R. Gassert, "Respiratory analysis during sleep using a chest-worn accelerometer: A machine learning approach," *Biomed. Signal. Proces.*, vol. 78, pp. 104014, 2022, doi: 10.1016/j.bspc.2022.104014.

[10] L.M. Dang, K. Min, H. Wang, M.J. Piran, C.H. Lee, and H. Moon, "Sensor-based and vision-based human activity recognition: A comprehensive survey," *Pattern Recogn.*, vol. 108, p. 107561, 2020, doi: 10.1016/j.patcog.2020.107561.

[11] Z. Zhang, Z. Wang, H. Lei, and W. Gu, "Gait phase recognition of lower limb exoskeleton system based on the integrated network model," *Biomed. Signal. Proces.*, vol. 76, p. 103693, 2022, doi: 10.1016/j.bspc.2022.103693.

[12] V.T. Van Hees *et al.* "Separating movement and gravity components in an acceleration signal and implications for the assessment of human daily physical activity," *Plos One*, vol. 8, no. 4, pp. e61691, 2013, doi: 10.1371/journal.pone.0061691.

[13] K.R. Vidyarani, V. Talasila, N. Megharjun, M. Supriya, K.R. Prasad, and G.R. Prashanth, "An inertial sensing mechanism for measuring gait parameters and gait energy expenditure," *Biomed. Signal. Proces.*, vol. 70, p. 103056, 2021, doi: 10.1016/j.bspc.2021.103056.

[14] Z. Zheng, Q. Wang, D. Deng, Q. Wang, and W. Huang, "CG-Recognizer: A biosignal-based continuous gesture recognition system," *Biomed. Signal. Proces.*, vol. 78, p. 103995, 2022, doi: 10.1016/j.bspc.2022.103995.

[15] S. Lambrecht, S.L. Nogueira, M. Bortole, A.A.G. Siqueira, M.H. Terra, E. Rocon, and J.L. Pons, "Inertial sensor error reduction through calibration and sensor fusion," *Sensors*, vol. 16, no. 2, p. 235, 2016, doi: 10.3390/s16020235.

[16] J.F.S. Lin and D. Kulić, "Human pose recovery using wireless inertial measurement units," *Physiol. Meas.*, vol. 33, no. 12, pp. 2099–2115, 2012, doi: 10.1088/0967-3334/33/12/2099.

[17] T.L. Baldi, F. Farina, A. Garulli, A. Giannitrapani, and D. Prattichizzo, "Upper Body Pose Estimation Using Wearable Inertial Sensors and Multiplicative Kalman Filter," *IEEE Sens.*, vol. 20, no. 1, pp. 492–500, 2019, doi: 10.1109/JSEN.2019.2940612.

[18] J.F.B. Ruiz, J.D. Chaparro, C.B. Peño, H.A.L. Solano, X.T. García and J.C. López, "A low-cost and unobtrusive system for fall detection," *Procedia Comput. Sci.*, vol. 192, pp. 2160–2169, 2021, doi: 10.1016/j.procs.2021.08.229.

[19] Y. Kim, H. Jung, B. Koo, J. Kim, T. Kim, and Y. Nam, "Detection of Pre-Impact Falls from Heights Using an Inertial Measurement Unit Sensor," *Sensors*, vol. 20, no. 18, p. 5388, 2020, doi: 10.3390/s20185388.

[20] T. Amasay, K. Zodrow, L. Kincl, J. Hess, and A. Karduna, "Validation of tri-axial accelerometer for the calculation of elevation angles," *Int. J. Ind. Ergonom.*, vol. 39, no. 5, pp. 783–789, 2009, doi: 10.1016/j.ergon.2009.03.005.

[21] K. Feng *et al.* "A new quaternion-based Kalman filter for real-time attitude estimation using the two-step geometrically-intuitive correction algorithm," *Sensors*, vol. 17, no. 9, p. 2146, 2017, doi: 10.3390/s17092146.

[22] W.H.K. De Vries, H.E.J. Veeger, C.T.M. Baten, and F.C.T. van der Helm, "Magnetic distortion in motion labs, implications for validating inertial magnetic sensors," *Gait Posture*, vol. 29, no. 4, pp. 535–541, 2009, doi: 10.1016/j.gaitpost.2008.12.004.

[23] N.H. Ariffin, N. Arsad, and B. Bais, " Low cost MEMS gyroscope and accelerometer implementation without Kalman Filter for angle estimation," in *Proc. 2016 International Conference*

on Advances in Electrical, Electronic and Systems Engineering. (ICAEES), 2016, pp. 77–82, doi: 10.1109/icaees.2016.7888013.

[24] J. Abbasi, H. Salarieh, and A. Alasty, "A motion capture algorithm based on inertia-Kinect sensors for lower body elements and step length estimation," *Biomed. Signal. Proces.*, vol. 64, p. 102290, 2021, doi: 10.1016/j.bspc.2020.102290.

[25] L. Xue, C.Y. Jiang, H.L. Chang, Y. Yang, W. Qin and W.Z. Yuan, "A novel Kalman filter for combining outputs of MEMS gyroscope array," *Measurement*, vol. 45, no. 4, pp. 745–754, 2012, doi: 10.1016/j.measurement.2011.12.016.

[26] P. Gui, L. Tang and S. Mukhopadhyay, "MEMS based IMU for tilting measurement: Comparison of complementary and Kalman filter based data fusion," in *Proc. 2015 IEEE 10th conference on Industrial Electronics and Applications. (ICIEA)*, 2015, pp. 2004–2009, doi: 10.1109/iciea.2015.7334442.

[27] C. Yi, J. Ma, H. Guo, J. Han, H. Gao, F. Jiang, and C. Yang, "Estimating three-dimensional body orientation based on an improved complementary filter for human motion tracking," *Sensors*, vol. 18, no. 11, p. 3765, 2018, doi: 10.3390/s18113765.

[28] G. Ligorio and A.M. Sabatini, "A novel Kalman filter for human motion tracking with an inertial-based dynamic inclinometer," *IEEE Trans. Biomed. Eng.*, vol. 62, no. 8, pp. 2033–2043, 2015, doi: 10.1109/TBME.2015.2411431.

[29] P. Promrit, S. Chokchaitam, and M. Ikura, " In-vehicle MEMS IMU calibration using accelerometer," in *Proc. 2018 IEEE 5th International Conference on Smart Instrumentation, Measurement and Application. (ICSIMA)*, 2018, pp. 1–3, doi: 10.1109/icsima.2018.8688778.

[30] R.G. Valenti, I. Dryanovski, and J. Xiao, "Keeping a good attitude: A quaternion-based orientation filter for IMUs and MARGs," *Sensors*, vol. 15, no. 8, pp. 19302–19330, 2015, doi: 10.3390/s150819302.

[31] R.G. Valenti, I. Dryanovski, and J. Xiao, "A linear Kalman filter for MARG orientation estimation using the algebraic quaternion algorithm," *IEEE T. Instrum. Meas.*, vol. 65, no. 2, pp. 467–481, 2015, doi: 10.1109/TIM.2015.2498998.

[32] S.O.H. Madgwick, " AHRS algorithms and calibration solutions to facilitate new applications using low-cost MEMS," PhD Thesis, University of Calgary, Canada, 2000.

[33] D.K. Shaeffer, "MEMS inertial sensors: A tutorial overview," *IEEE Commun. Mag.*, vol. 51, no. 4, pp. 100–109, 2013, doi: 10.1109/MCOM.2013.6495768.

[34] H.W. Hsu, T.Y. Wu, S. Wan, W.H. Wong and C.Y. Lee, "QuatNet: Quaternion-Based Head Pose Estimation With Multiregression Loss," *IEEE Trans. Multimedia*, vol. 21, no. 4, pp. 1035–1046, 2018, doi: 10.1109/TMM.2018.2866770.

[35] H. Guo and H. Hong, "Research on filtering algorithm of MEMS gyroscope based on information fusion," *Sensors*, vol. 19, no. 16, pp. 3552, 2019, doi: 10.3390/s19163552.

[36] C. Kownacki, "Optimization approach to adapt Kalman filters for the real-time application of accelerometer and gyroscope signals' filtering," *Digit. Signal. Process.*, vol. 21, no. 1, pp. 131–140, 2011, doi: 10.1016/j.dsp.2010.09.001.

[37] P. Schober, C. Boer and L.A. Schwarte, "Correlation coefficients: appropriate use and interpretation," *Anesth. Analg.*, vol. 126, no. 5, pp. 1763–1768, 2018, doi: 10.1213/ANE.0000000000002864.

[38] N. Jalloul, "Wearable sensors for the monitoring of movement disorders," *Biomed. J.*, vol. 41, no 4, pp. 249–253, 2018, doi: 10.1016/j.bj.2018.06.003.

[39] F.J. Ordóñez and D. Roggen, "Deep Convolutional and LSTM Recurrent Neural Networks for Multimodal Wearable Activity Recognition," *Sensors*, vol. 16, no. 1, p. 115, 2016, doi: 10.3390/s16010115.